Robustness Margins for Linear Parameter Varying Systems

Ann-Kathrin Schug*, Peter Seiler and Harald Pfifer
Hamburg University of Technology, University of Minnesota, University of Nottingham

Aerospace Lab
Special issue on design & validation of aerospace control systems

Draft, July 2016.

Abstract

An approach to extend classical robustness margins to linear parameter varying (LPV) systems is presented. LPV systems are often used to model aircraft dynamics that are highly dependent on the operating conditions such as altitude and airspeed. Classical gain and phase margins are evaluated in the frequency domain and therefore cannot be applied to LPV systems. The proposed approach is based on a time-domain interpretation for disk margins. Specifically, a norm bounded linear time invariant (LTI) uncertainty is interconnected to the nominal LPV system. Next, a time-domain worst-case metric is applied to evaluate both the robustness margin and also the robust performance degradation. The approach does not require detailed uncertainty modeling. In addition, the analysis can be formulated as a convex optimization leading to reliable numerical analysis tools. As an example, the LPV gain margin of a flutter suppression controller for a flexible aircraft is evaluated.

1 Introduction

This paper presents a method to extend the notion of classical stability margins to linear parameter varying (LPV) systems. Classical gain and phase margins are widely used as a standard formulation for robustness requirements in the aerospace industry, see Section 2. They do not require specific, detailed uncertainty models and hence these margins are easy to evaluate. Additionally, engineers have significant experience on the interpretation of the analysis results. At the same time, gain scheduling is a commonly used design method in aerospace. Since the classical margins are evaluated in the frequency domain, they cannot be directly applied to LPV systems due to the time varying nature of the dynamics. It is typical to simply evaluate the margins at "frozen" flight conditions. However this fails to capture the effects of varying flight conditions. This motivates the proposed generalized robustness margins for LPV systems. The approach presented in this section provides two main extensions to the classical margins. A time domain worst-case metric can be used to formulate a generalized robustness margin for LPV systems, see Section 3. Additionally, this approach also considers the performance degradation before instability occurs.

Recently, the usage of a general uncertainty framework, namely integral quadratic constraints (IQCs) [6], have gained a lot of attention in the aerospace field [16, 4]. The main focus of this research has been the studying of the effects of complex uncertain or nonlinear elements, e.g., saturations. Still, these methods focus on assessing robustness over a set of "frozen" flight conditions. In contrast, this work builds on novel techniques that extend the IQC framework to LPV systems [10, 11]. This new approach builds on a time domain interpretation of IQCs and the dissipation inequality framework. An LPV equivalent to classical disk margins can be formulated in this framework. It retains the main characteristic of LTI disk margins. Specifically, at a frozen

*Corresponding A. Schug: ann.schug@tuhh.de

parameter value it guarantees robustness against a simultaneous gain and phase variations. It is anticipated that an engineer's previous experience with classical margins is directly applicable to this novel formulation. It shall be emphasized that it only requires a simple uncertainty element, i.e. norm-bounded uncertainty that describes the disk margin. Hence, the approach suits itself to complex systems, e.g. the analysis of a flutter suppression controller for a flexible aircraft as shown in Section 4

There are several recent robust performance results obtained for LPV systems whose state matrices have rational dependence on the scheduling parameters, e.g., [13]. In contrast, the results in this paper are for the class of LPV systems whose state matrices have an arbitrary dependence on the parameters. This is the natural modeling framework in aerospace applications, where LPV models are generally obtained by linearization of nonlinear systems.

2 Background

In many aerospace applications the dynamics strongly depend on the operating conditions of the aircraft such as altitude or airspeed. The LPV framework can be used to consider this dependency in the modeling procedure as well as the controller synthesis. The dynamics are expressed as a function of a scheduling parameter. This section provides a brief summary of LPV modeling and introduces the performance of nominal LPV systems. This work aims to extend classical (LTI) robustness margins and robust performance analysis to LPV systems. The approach is based on the concept of disk margins for LTI systems as reviewed in Section 2.2.

2.1 Linear Parameter Varying Systems

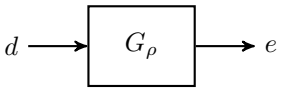

Figure 1: LPV System

Linear parameter varying (LPV) systems are a special class of time varying systems where the dynamics depend on an exogenous parameter vector $\rho(t)$ restricted to remain in a compact set $\rho(t) \in \mathcal{P} \subset \mathbb{R}^{n_\rho}$ for all $t \geq 0$. An n^{th}-order LPV system G_ρ as depicted in Figure 1 has the form

$$\begin{aligned} \dot{x}(t) &= A(\rho(t))\, x(t) + B(\rho(t))\, d(t), \\ e(t) &= C(\rho(t))\, x(t) + D(\rho(t))\, d(t), \end{aligned} \tag{1}$$

with the continuous functions $A : \mathbb{R}^{n_\rho} \to \mathbb{R}^{n_x \times n_x}, B : \mathbb{R}^{n_\rho} \to \mathbb{R}^{n_x \times n_d}, C : \mathbb{R}^{n_\rho} \to \mathbb{R}^{n_e \times n_x}$ and $D : \mathbb{R}^{n_\rho} \to \mathbb{R}^{n_e \times n_d}$. In addition, $x(t) \in \mathbb{R}^{n_x}$ is the vector containing the states of the system, $e(t) \in \mathbb{R}^{n_y}$ is the output vector and $d(t) \in \mathbb{R}^{n_u}$ the input vector. Given by the physical restrictions of most practical applications the admissible parameter trajectories are defined by

$$\mathcal{A} := \{\rho : \mathbb{R}^+ \to \mathbb{R}^{n_\rho} | \rho(t) \in \mathcal{P},\, \dot{\rho}(t) \in \dot{\mathcal{P}} \;\forall\; t \geq 0\} \tag{2}$$

where the admissible parameter rate is given by the subset

$$\dot{\mathcal{P}} := \{\dot{\rho} \in \mathbb{R}^{n_\rho} \mid |\dot{\rho}_i| \leq \nu_i,\, i = 1, \ldots, n_\rho\},$$

ν_i is the fastest admissible parameter variation rate.

The performance of an LPV system G_ρ can be measured in terms of the induced $\mathcal{L}_2$-norm. First define the norm of a signal d as $\|d\|_2 = \sqrt{\int_0^\infty d^T(t) d(t)\, dt}$. The set of bounded signals, i.e.

$d \in \mathcal{L}_2$, are those that satisfy $\|d\|_2 < \infty$. The gain of the system from the input d to the output e can be defined using the signal $\mathcal{L}_2$-norm:

$$\|G_\rho\| := \sup_{0 \neq d \in \mathcal{L}_2, \rho \in \mathcal{A}, x(0)=0} \frac{\|e\|_2}{\|d\|_2} \tag{3}$$

A bounded-real type result exists to bound the induced $\mathcal{L}_2$-norm of an LPV system. First, define the following differential operator for a symmetric matrix function $P : \mathcal{P} \to \mathbb{S}^{n_x}$:

$$\partial P(\rho, \dot{\rho}) = \sum_{i=1}^{n_\rho} \frac{\partial P(\rho)}{\partial \rho_i} \dot{\rho}_i, \tag{4}$$

The theorem below provides a matrix inequality condition to prove stability and bound the induced $\mathcal{L}_2$ gain of an LPV system with bounded parameter variation rate.

Theorem 2.1 (Bounded Real Lemma [19]) *An LPV System G_ρ as defined in* (1) *is exponentially stable and $\|G_\rho\| < \gamma$ if there exists a continuously differentiable symmetric matrix function $P : \mathcal{P} \to \mathbb{S}^{n_x}$ such that the following two conditions hold $\forall (\rho, \dot{\rho}) \in \mathcal{P} \times \dot{\mathcal{P}}$*

$$P(\rho) > 0, \tag{5}$$

$$\begin{bmatrix} P(\rho)A(\rho) + A(\rho)^T P(\rho) + \partial P(\rho, \dot{\rho}) & P(\rho)B(\rho) \\ B(\rho)^T P(\rho) & -I \end{bmatrix} + \frac{1}{\gamma^2} \begin{bmatrix} C(\rho)^T \\ D(\rho)^T \end{bmatrix} \begin{bmatrix} C(\rho) & D(\rho) \end{bmatrix} < 0. \tag{6}$$

Proof. This is a standard result but a sketch of the proof is provided as it will be extended for the robustness result. Multiply (6) on the left and right by $\begin{bmatrix} x^T, d^T \end{bmatrix}$ and $\begin{bmatrix} x^T, d^T \end{bmatrix}^T$ respectively to obtain (neglecting the dependence on time):

$$\dot{x}^T P(\rho) x + x^T P(\rho) \dot{x} + x^T \partial P(\rho, \dot{\rho}) x + \frac{1}{\gamma^2} e^T e - d^T d < 0. \tag{7}$$

Define a storage function $V : \mathbb{R}^{n_x} \times \mathcal{P} \to \mathbb{R}^+$ as $V(x, \rho) = x^T P(\rho) x$. Evaluating V along the state and parameter trajectory gives

$$\dot{V} + \frac{1}{\gamma^2} e^T e - d^T d < 0. \tag{8}$$

Integrating over the time interval $[0, T]$ and applying $x(0) = 0$ yields

$$V(T) + \frac{1}{\gamma^2} \int_0^T e(t)^T e(t) dt - \int_0^T d(t)^T d(t) dt < 0. \tag{9}$$

Let $T \to \infty$ and use $V(T) \geq 0$ as well as the definition of the $\mathcal{L}_2$-norm to obtain bound $\|e\|_2 \leq \gamma \|d\|_2$. A slight modification of the arguments (using the compactness of $\mathcal{P}$) yields the strict inequality $\|e\|_2 < \gamma \|d\|_2$.

□

2.2 Disk Margins for LTI Systems

In many applications it is important to provide a high level of robustness. Specifically, the system performance should be insensitive to deviations between the model used for the controller synthesis and the actual system dynamics. Classical robustness measures, e.g.gain and phase margins, can be easily evaluated given the frequency response of the nominal system dynamics. More modern tools, e.g. μ analysis, require more detailed descriptions of the uncertainty. In general, an uncertain system can be described by "pulling out the uncertainty" as shown in Figure 2 [20]. This corresponds to an interconnection of a nominal (not-uncertain) system G and an uncertainty block Δ. The signals d and e correspond to exogenous inputs and system outputs, respectively.

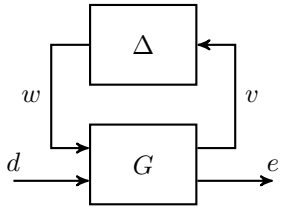

Figure 2: Uncertain LTI System

The signals v and w correspond to the signals related to the modeled uncertainty. The notation $F_u(G, \Delta)$ is used to represent this interconnection structure.

As noted above, classical gain and phase margins are common robustness metrics. These margins measure the amount of (individual) gain or phase that can be tolerated before a single closed-loop becomes unstable. On the other hand, symmetric disk margins, as described in [3, 1], allow for simultaneous variations in both gain and phase within a prescribed disk. The remainder of the section briefly reviews the disk margin concept as this will be used to formulate the proposed robustness margins for LPV systems. Consider the interconnection shown in Figure 3 where G and K are single input / single output (SISO) LTI systems and Δ is an LTI uncertainty. The symmetric disk margins are related to robustness with respect to this uncertainty interconnection.

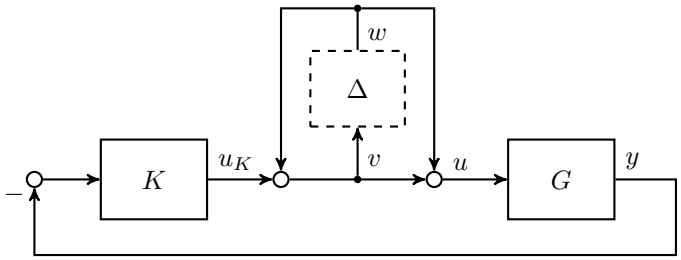

Figure 3: Input Disk Margin Interconnection

The open loop transfer function, without Δ, from input w to output v is given by $\frac{1}{S_i - T_i}$ where $S_i := \frac{1}{1+GK}$ and $T_i := \frac{GK}{1+GK}$ are the sensitivity and complementary sensitivity functions at the plant input. Thus the disk margin interconnection is equivalent to $F_u(\frac{1}{S_i - T_k}, \Delta)$ (with no disturbance and error channels). By the small gain theorem [5, 20], the uncertain disk margin interconnection is stable if and only if $\|\Delta\|_\infty < \|\frac{1}{S_i - T_i}\|_\infty$. Thus the stability radius (margin) can be defined as $r := 1/\|S_i - T_i\|$ where r typically satisfies $0 < r < 1$.

Block diagram manipulation can be used to bring the disk margin interconnection into the equivalent form shown in Figure 4. The alternative form provides a useful connection back to classical gain and phase margins. This implies that the interconnection is stable for all real gains from u_K to u in the interval $\left[\frac{1-r}{1+r}, \frac{1+r}{1-r}\right]$. This proves the following symmetric lower and upper disk gain margins:

$$\mathrm{GM}_l = \frac{1-r}{1+r}, \quad \mathrm{GM}_u = \frac{1+r}{1-r}. \tag{10}$$

Similarly, stability of Figure 4 for all $\|\Delta\|_\infty < r$ can be used to show that the loop is stable for additional phase (from u_K to u) within the following disk phase margin limits:

$$\mathrm{PM}_l = -2\cot(r), \quad \mathrm{PM}_u = 2\cot(r). \tag{11}$$

These are called disk margins due to a connection in the Nyquist domain. Specifically, stability of the interconnection in Figure 4 for all $\|\Delta\|_\infty < r$ implies the open loop Nyquist curve of GK stays outside the disk containing -1 and with diameter passing through $[-\mathrm{GM}_u, -\mathrm{GM}_l]$. Figure 5 shows the disk margins for an example transfer function. The critical point (-1,0) is marked in

red. The interval on the real axis between the disk (orange) and the critical point corresponds to the gain margin and the intersection of the disk and the circle around the origin with radius 1 marks the arc of the phase margin. For further information on disk margins the reader is referred to e.g. [3].

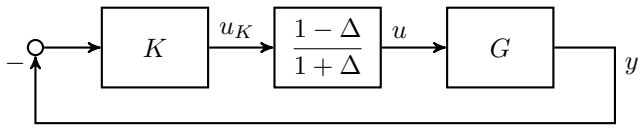

Figure 4: Equivalent Input Disk Margin Interconnection

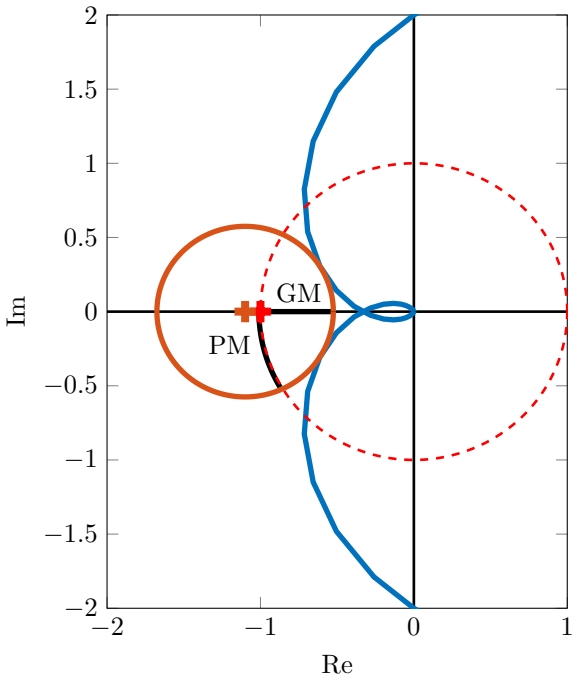

Figure 5: Disk Margin in the Nyquist Plane

3 LPV Robustness Margins

This section extends the disk margin defined in the previous section to LPV systems. At a frozen parameter value, it retains the frequency domain interpretation given above. However, it is derived completely in the time domain. This allows using disk margins to consider the time varying nature of gain scheduled controllers.

3.1 LPV Disk Margins

The generalized disk margin interconnection in Figure 6 will be used for the analysis. This contains two significant differences from the previous disk margin interconnection in Figure 3. First, the plant G_ρ and controller K_ρ are allowed to be LPV systems. Here ρ is a parameter vector defining the flight condition. Second, an input d and output e are added in order to consider performance criteria. This corresponds to a plant input disturbance and plant output error. More generally, performance inputs/outputs can be included at any point in the feedback diagram depending on the specific application.

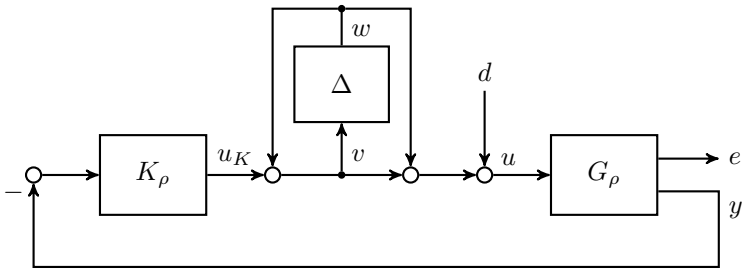

Figure 6: Input Disk Margin Interconnection for LPV Systems

It is common to evaluate the classical margins with G_ρ and K_ρ evaluated at specific grid points of ρ. With a constant ρ both the plant and controller are then LTI systems at the fixed operating condition. The disk margin analysis presented in Section 2.2 can be directly applied to this LTI interconnection. However, the resulting analysis does not consider the actual time varying nature of ρ. The approach proposed in this paper directly deal with the time varying operating conditions using the framework developed in [10].

Two basic robustness analysis problems will be considered based on the LPV interconnection in Figure 6:

1. **LPV Disk Margins**: Let Δ be an LTI uncertainty. Compute a stability margin r such that the LPV interconnection is stable for all $\|\Delta\|_\infty < r$ and all $\rho \in \mathcal{A}$.

2. **Worst-Case Gain**: Again let Δ be an LTI uncertainty. In addition, assume the uncertainty satisfies a given norm-bound $b < r$, i.e. $\|\Delta\|_\infty < b$. Compute the worst-case gain from d to e over this set of uncertainties and and all $\rho \in \mathcal{A}$.

The analysis requires a time-domain characterization of the uncertainty. Let $w = \Delta(v)$ where both w and v are assumed to be scalar signals to simplify this discussion. The norm-bound $\|\Delta\|_\infty < b$ implies the following frequency-domain constraint on the input-output signals:

$$\int_{-\infty}^{\infty} b^2|V(j\omega)|^2 - |W(j\omega)|^2\, d\omega = \int_{-\infty}^{\infty} V(j\omega)^* \left(b^2 - \Delta(j\omega)^*\Delta(j\omega)\right) V(j\omega)\, d\omega \geq 0 \qquad (12)$$

where $V(j\omega)$ and $W(j\omega)$ are the transforms of the signals $v(t)$ and $w(t)$. By Parseval's theorem [20], this inequality is equivalent to an infinite-horizon, time-domain constraint:

$$\int_0^{\infty} \begin{bmatrix} v(t) \\ w(t) \end{bmatrix}^T \begin{bmatrix} b^2 & 0 \\ 0 & -1 \end{bmatrix} \begin{bmatrix} v(t) \\ w(t) \end{bmatrix} dt \geq 0. \qquad (13)$$

The causality of Δ implies that this constraint also holds for all finite intervals $[0, T]$, for all $v \in \mathcal{L}_2$, $w = \Delta(v)$ and $T > 0$ [10]. The time-invariance of Δ can be used to formulate a tighter constraint as is standard in structured singular value (μ) analysis [12, 7]. Specifically, Δ is LTI and hence it commutes with any stable, minimum-phase LTI system D, i.e. $D(s)\Delta(s) = \Delta(s)D(s)$. This property is the basis for the use of frequency-domain "D"-scale conditions in μ analysis [12, 7]. The equivalent time-domain formulation is obtained by noting that if $w = \Delta v$ then $Dw = \Delta Dv$. Hence the filtered signals $(\tilde{v}, \tilde{w}) := (Dv, Dw)$ satisfy the same norm bound constraints as (v, w). To simplify notation, combine the scalings D and stack the filtered signals as follows:

$$z := \begin{bmatrix} \tilde{v} \\ \tilde{w} \end{bmatrix} = \Psi \begin{bmatrix} v \\ w \end{bmatrix} \text{ where } \Psi := \begin{bmatrix} D & 0 \\ 0 & D \end{bmatrix} \qquad (14)$$

As noted above, the filtered signals $(\tilde{v}, \tilde{w}) := (Dv, Dw)$ satisfy the same norm bound constraints as (v, w). This leads to the following time-domain inequality.

Definition 3.1 *Let Δ be an LTI system satisfying $\|\Delta\|_\infty < b$. In addition, let D be a stable, minimum phase LTI system. Define Ψ as in Equation 14 and $M = \left[\begin{smallmatrix} b^2 & 0 \\ 0 & -1 \end{smallmatrix}\right]$. Then Δ satisfies*

$$\int_0^T z(t)^T M z(t) dt \geq 0. \tag{15}$$

for all $v \in \mathcal{L}_2, w = \Delta(v)$ and $T \geq 0$.

Equation 15 is a specific example of a time-domain *Integral Quadratic Constraint* (IQC). IQCs provide a general framework, introduced in [6], for studying various uncertainties such as infinite dimensional systems or hard non-linearities. There is an existing library of IQCs (Ψ, M) for particular classes of uncertainties. The (Ψ, M) given in Definition 3.1 is for the particular class of LTI, norm-bounded uncertainty. The more general IQC framework can be used to obtain worst-case stability margins for other cases, e.g. systems with saturation. However, this paper will focus on norm bounded, LTI uncertainties in order to assess LPV disk margins.

3.2 LPV Worst-Case Gain

The (nominal) stability conditions of Section 2.1 can now be combined with the time domain constraint on the input/output behavior of the uncertainty block Δ. This can be used to assess the robust performance of an uncertain LPV system. First note that the LPV disk margin interconnection (Figure 6) is a special instance of the more general uncertain LPV system interconnection in Figure 7. Here the nominal (not uncertain) LPV system T_ρ is connected to the uncertainty block. In addition the dynamic filter Ψ, used to describe the IQC in Definition 3.1, is also appended to the diagram. The combined dynamics of T_ρ and Ψ are described by the following LPV system:

$$\begin{array}{rcllll} \dot{x} & = & A(\rho)x & +B_1(\rho)w & +B_2(\rho)d \\ z & = & C_1(\rho)x & +D_{11}(\rho)w & +D_{12}(\rho)d \\ e & = & C_2(\rho)x & +D_{21}(\rho)w & +D_{22}(\rho)d \end{array} \tag{16}$$

The state vector combines the state of T_ρ and the state of Ψ, i.e. $x = \left[x_{T_\rho}^T, x_\Psi^T\right]^T$. The perturbation block Δ is unknown and is not considered for the purposes of analysis. Instead, w is treated as external signal subject to the constraint on z given in Equation 15. This effectively replaces the precise relation $w = \Delta(v)$ by the imprecise time domain inequality.

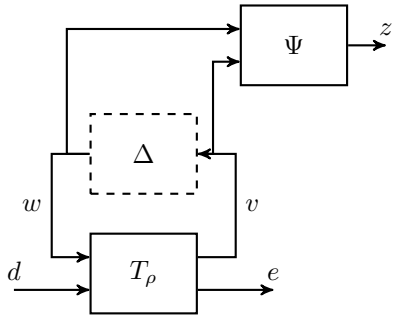

Figure 7: Worst-Case Gain Analysis Interconnection

The robust performance of this general uncertain LPV system (Figure 7) can be measured by the worst-case induced $\mathcal{L}_2$ gain from input d to output e over all uncertainties Δ satisfying the finite-time horizon constraint in (15). The following theorem (from [10]) provides a matrix inequality condition to compute the upper bound on the worst case $\mathcal{L}_2$-gain of $\mathcal{F}_u(T_\rho, \Delta)$.

Theorem 3.2 (Extended Bounded Real Lemma [10]) *Let $\mathcal{F}_u(T_\rho, \Delta)$ be well posed for any $\Delta \in IQC(\Psi, M)$. Then the worst case gain of $F_u(T_\rho, \Delta)$ is upper bounded by $\gamma < \infty$ if there exists*

a continuously differentiable $P : \mathcal{P} \to \mathbb{S}^{n_x}$ *and a scalar* $\lambda > 0$ *such that the following conditions hold for all* $(\rho, \dot{\rho}) \in \mathcal{P} \times \dot{\mathcal{P}}$*:*

$$P(\rho) > 0, \tag{17}$$

$$\begin{bmatrix} P(\rho)A(\rho) + A(\rho)^T P(\rho) + \partial P(\rho,\dot{\rho}) & P(\rho)B_1(\rho) & P(\rho)B_2(\rho) \\ B_1(\rho)^T P(\rho) & 0 & 0 \\ B_2(\rho)^T P(\rho) & 0 & -I \end{bmatrix}$$

$$+\lambda \begin{bmatrix} C_1(\rho)^T \\ D_{11}^T(\rho)^T \\ D_{12}^T(\rho)^T \end{bmatrix} M \begin{bmatrix} C_1(\rho) & D_{11}(\rho) & D_{12}(\rho) \end{bmatrix} \tag{18}$$

$$+\frac{1}{\gamma^2} \begin{bmatrix} C_2(\rho)^T \\ D_{21}(\rho)^T \\ D_{22}(\rho)^T \end{bmatrix} \begin{bmatrix} C_2(\rho) & D_{21}(\rho) & D_{22}(\rho) \end{bmatrix} < 0$$

Proof. The proof is similar to Theorem 2.1. The uncertainty Δ is assumed to satisfy the IQC defined by (Ψ, M) and therefore the signal z satisfies (15) for any $T > 0$. Define a storage function $V(x, \rho) = x^T P(\rho) x$ as in the proof of Theorem 2.1. Left/right multiplication of Equation 18 by $\left[x^T, w^T, d^T\right]$ and $\left[x^T, w^T, d^T\right]^T$ leads to the following dissipation inequality

$$\dot{V} - d^T d + \lambda z^T M z + \frac{1}{\gamma^2} e^T e < 0 \tag{19}$$

Integrating (19) over the finite time horizon $[0, T]$ and using the initial condition $x(0) = 0$ along with the conditions $\lambda > 0$ and $P(\rho) > 0$ leads to the gain bound $\|e| \leq \gamma \|d\|$. This holds for any input $d \in \mathcal{L}_2$, admissible parameter trajectory $\rho \in \mathcal{A}$ and uncertainty $\Delta \in IQC(\Psi, M)$. Therefore the worst-case gain is upper bounded by γ.

□

If the linear matrix inequality (LMI) conditions in Theorem 3.2 are feasible, then the system is stable for the selected uncertainty bound b. A bisection can be used to find the largest value of b for which the LMI is feasible. This largest uncertainty bound corresponds to the stability (disk) margin, denoted r, for the LPV system. For example, the interconnection in Figure 6 is stable for all real gains all real gains from u_K to u in the interval $\left[\frac{1-r}{1+r}, \frac{1+r}{1-r}\right]$. The other disk margin interpretations given in Section 2.2 have similar extensions to the LPV interconnection. The key point is that the plant and controller are LPV and the time-domain analysis enables the robustness with respect to LTI (disk-margin) uncertainty to be evaluated.

Theorem 3.2 can also be used to evaluate performance in addition to the stability margin. In particular it is important to emphasize that the performance can become unacceptable before the system becomes unstable. Thus it is useful to evaluate the performance degradation for uncertainty bounds within the stability margin. In other words, a plot of worst-case gain vs. uncertainty bound b will approach infinity as $b \to r$. The performance degradation as the bound b increases provides additional useful information beyond simply knowing the stability margin r. It should also be mentioned that this approach can be used to obtain generalized delay margins for LPV systems using existing time-domain IQCs for time delays. The work in [9] provides detailed information on IQCs for time-delayed LPV systems.

3.3 Numerical Implementation

The conditions in Theorem 3.2 involve infinite dimensional LMIs, i.e. the conditions must hold for all $\rho \in \mathcal{P}$. An approximation based on gridding is proposed in [18]. Specifically, the parameter space is approximated by a finite grid over $(\mathcal{P} \times \dot{\mathcal{P}})$. The system in (1) is then evaluated at each grid point. The LMI conditions in Theorem 3.2 are enforced only at the grid points leading to finite dimensional linear matrix inequalities. Since the conditions depend affinely on the parameter rate it is sufficient to enforce them only at the rate bounds $\pm\nu_i$. Thus no gridding over $\dot{\mathcal{P}}$ is needed.

It should be emphasized that this gridding is only an approximation. Feasibility of the LMIs on a finite grid does not guarantee feasibility for all $\mathcal{P}$. However, the gridding approximation is often sufficient on practical problems. Typically the process is to solve the LMIs on a coarse grid and then to verify the results on a denser grid.

Another issue is that the matrix function P in Theorem 3.2 is itself parameter dependent. This function P can be expanded in terms of a finite number of basis functions

$$P(\rho) = \sum_{j}^{n_\rho} b_j(\rho) P_j, \tag{20}$$

where $b_j : \mathbb{R}^{n_\rho} \to \mathbb{R}$ can be any user-defined differentiable basis functions. The matrices P_j appearing in this expansion describe the function P with a (finite) number of decision variables.

The final issue is the description of the IQC which involves the scaling D. In μ-analysis the search over the D-scales is performed in the frequency domain on a grid of frequencies. This approach cannot be replicated for LPV analysis as the condition in Theorem 3.2 is formulated in the time domain. Instead, many different D-scales, e.g. $\{D_i\}_{i=1}^N$ can be selected. Each D_i defines a valid IQC with corresponding filter Ψ_i. The LMI conditions in Theorem 3.2 can be augmented in order to handle these multiple dynamic filters Ψ_i. The extended system then includes the additional dynamics of all Ψ_i. The corresponding LMI condition in (18) is modified to include one term corresponding to each selected D_i:

$$\sum_{i=1}^{N} \lambda_i \begin{bmatrix} C_{1i}(\rho)^T \\ D_{11i}(\rho)^T \\ D_{12i}(\rho)^T \end{bmatrix} M_i \begin{bmatrix} C_{1i}(\rho) & D_{11i}(\rho) & D_{12i}(\rho) \end{bmatrix} \tag{21}$$

The constants λ_i are decision variables each of which must be ≥ 0. The output state matrices $(C_{1i}(\rho), D_{11i}(\rho), D_{12i})$ corresponding to the output z_i of filter Ψ_i. The analysis includes a search for the constants λ_i that lead to the feasibility of the LMI conditions in Theorem 3.2. It is worth noting that, in principle, Ψ and M do not have to be LTI but could potentially be LPV. However, the use of LPV (Ψ, M) has not be fully developed in the literature and will not be pursued here.

4 Application on a Flexible Aircraft

The proposed method is used to evaluate the LPV robustness margins of an flutter suppression controller of a flexible aircraft. The airframe is a small, radio-controlled aircraft denoted mini-MUTT, as shown in Figure 8. The design is based on Lockheed Martins Body Freedom Flutter vehicle [2]. The mini-Mutt has a mass of 6.7 kg and a wing span of 3 meters. It was build completely in-house at the University of Minnesota to study the usage of active control to suppress detrimental structural and aerodynamic interactions. These undesired interactions lead to a phenomenon called flutter which is an unstable oscillation that can potentially destroy the aircraft. Given the catastrophic consequences of flutter, it is paramount to have an insightful and accurate robustness metric available.

4.1 System Description

The modeling of the aircraft incorporates structural and rigid body dynamics as well as aerodynamics. The procedure can be found in [14]. The final model which is used is adapted from [8] and describes the longitudinal dynamics for straight and level flight. The system has a total of six states as well as one input and three output signals.

A schematic overview of the aircraft is depicted in Figure 9 showing the available sensors and actuators. The aircraft has a total of 8 flaps on the back of the wing. The body flaps are unused in this example while the inner two are aileron and elevator respectively. The flutter suppression controller has full authority over the outboard flap deflection denoted by δ, such that $u = \delta$. The plant output signals are the pitch rate q and the vertical acceleration at the center of gravity a_{CG}

Figure 8: mini-MUTT

and the wing tips a_{WT}, such that $y = [q\, a_{CG}\ a_{WT}]$. A 4^{th}-order short period approximation of the full model as proposed in [15] is used. The first two states of the state space representation are associated to the rigid body dynamics and consist of the angle of attack α and pitch rate q. The remaining states represent the generalized displacement and velocity of the first flexible mode, denoted by η and $\dot{\eta}$ respectively. Therefore, the approximated plant model is of 4^{th}-order and consists of the four states $\alpha, q, \eta, \dot{\eta}$. The dynamics strongly depend on the airspeed and it is therefore straightforward to represent the aircraft model as a parameter varying model. Specifically, the airspeed is assumed to be a measurable exogenous signal which can be used as the scheduling parameter parameter $\rho(t)$. Additionally, the sensor and actuator dynamics and the assumed time delay as described in[15] are included, leading to the final 6^{th}-order LPV model.

The LPV controller is mainly based on the H_∞ design which is also proposed in [15]. In this work the airspeed is assumed to be constant 30 m/s. To adapt the controller design to the LPV description of the system, the loopshaping approach can be systematically extended using the

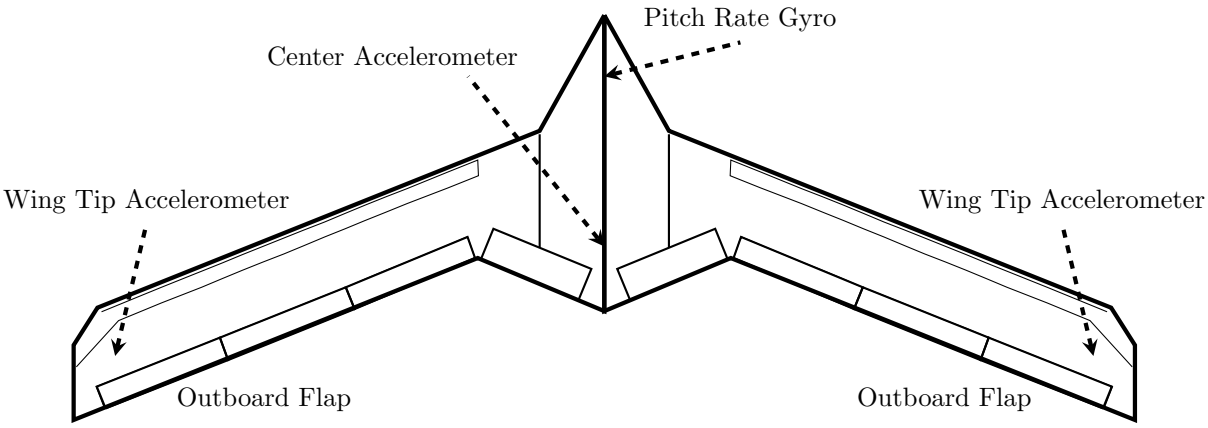

Figure 9: Schematic Overview

synthesis algorithm provided in [19]. Weighting filters can be used to shape the individual transfer functions of the performance channels. The modal velocity $\dot{\eta}$ of the first flexible mode is used as a non-measurable performance output. Since the main objective of the flutter suppression controller is to attenuate the mode, this can be achieved by pushing down the peak in the associated transfer function using a constant weighting filter.

4.2 Robustness Analysis

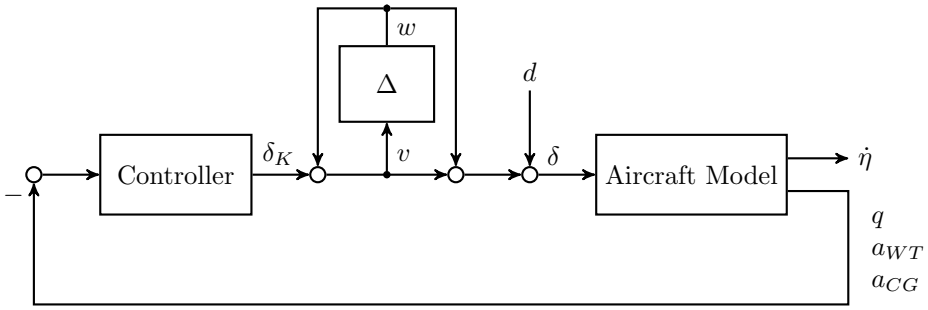

Figure 10: Equivalent Input Disk Margin Interconnection

The LPV robustness margin analysis is performed on the closed-loop system of the aircraft and the LPV flutter suppression controller as shown in Figure 10. The parameter range is assumed to be $\rho = [20, \ldots, 40]$ m/s and the parameter variation rate is bounded by ± 10 m/s^2. The worst-case performance is computed for increasing values of b by solving the LMI conditions in Theorem 3.2. The results are then normalized by the $\mathcal{L}_2$ gain of the nominal system ($b = 0$). Recall, that a norm bounded uncertainty is assumed to satisfy an IQC of the form

$$\Psi_1 = I_2, \qquad M = \begin{bmatrix} b^2 & 0 \\ 0 & -1 \end{bmatrix}. \tag{22}$$

A second filter with simple dynamics

$$\Psi_2 = \begin{bmatrix} \dfrac{1}{s+1} & 0 \\ 0 & \dfrac{1}{s+1} \end{bmatrix} \tag{23}$$

is added to the analysis. Initially, a constant matrix function P is used for the LMI conditions in Theorem 3.2. The analysis is then repeated, using linear and quadratic basis functions for the approximation of $P(\rho)$, i.e. $P(\rho) = P_0 + \rho P_1$ and $P(\rho) = P_0 + \rho P_1 + \rho^2 P_2$.

Evaluation

The analysis results using quadratic basis functions are shown in Figure 11. The optimization algorithm could not find any feasible solutions using a constant P and a linear basis functions. Hence, only the analysis using quadratic storage functions if shown in the figure. Adding an additional IQC with internal dynamics shows only minimal improvement of the results. As a comparison, a lower bound of the disk margin is computed based on the μ-Analysis framework. Specifically, at each frozen value ρ and each value of b, the Matlab function `wcgain` is used to compute LTI worst-case gain. The largest gain of all grid points is then plotted as a function of the uncertainty norm bound b, labeled LTI in Fig. 11.

The grey dashed line in the figure is the LPV disk margin, i.e. the uncertainty bound at which no stability can be guaranteed. The upper bound for the LPV robustness margin in the given example is $b_{max} \approx 0.27$, corresponding to a real gain at the plant input of about 1.7 (4.6 dB). As a comparison, the lowest LTI input-disk margin over all individual grid points is 4.9 dB. As

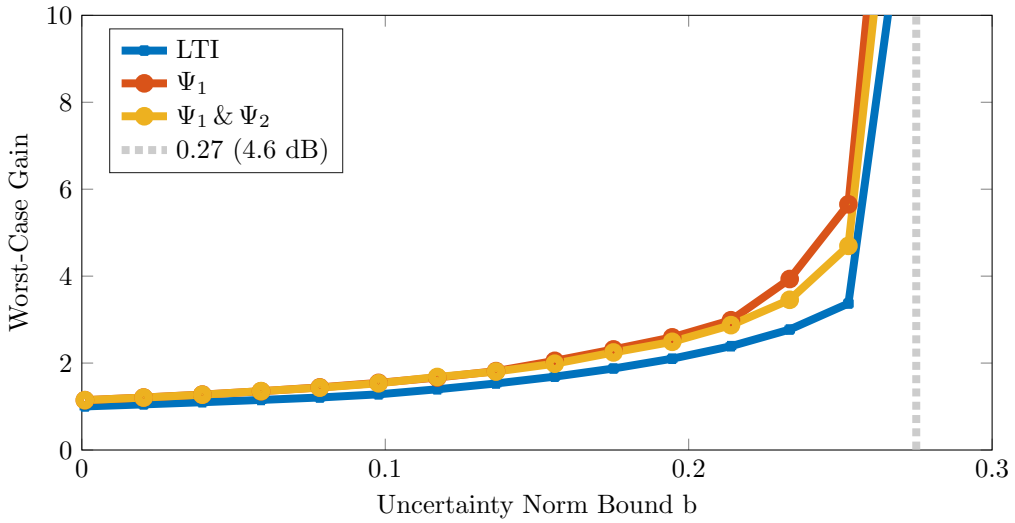

Figure 11: Norm Bounded Uncertainty Worst-Case Gain

mentioned previously, this is only a single number. While it gives some insight on the robustness of the controller, additional insight can be gained by considering the performance degradation. The gain at $b = 0$ is the nominal performance of the system and is used as a reference for the robustness performance analysis. The degradation can be interpreted in the following way. The performance of the controller is already degraded by a factor of two at an uncertainty $b \approx 0.18$ and by a factor of three at $b \approx 0.23$. This performance degradation is a valuable metric for controller evaluation. In many practical aerospace applications, stabilization is not sufficient for the safe operation and some level of performance is required.

Note that in this example the lower bounds computed via `wcgain` are close to the upper bounds on the worst-case gain for the uncertain LPV system. In general, the gap between both methods can be large. Recall, that `wcgain` is only an LTI analysis at each (frozen) grid point. The LPV analysis maximizes the gain over all allowable parameter trajectories while the `wcgain` analysis can be viewed as restricting the trajectory to be frozen at a single parameter value.

5 Conclusion

A novel approach to extend classical disk margins to LPV systems has been proposed. It allows the analysis of gain-scheduled controller which is the predominant control architecture in aerospace. Unlike classical margins, the proposed margin incorporates the time variations in the analysis. The problem is formulated as a convex optimization which can be readily solved even for complex systems. The applicability was demonstrated on a flutter suppression controller for a flexible, unmanned aircraft.

Acknowledgments

This work is supported by the NASA NRA Cooperative Agreement under Grant No. NNX14AL36A, entitled “Lightweight Adaptive Aeroelastic Wing for Enhanced Performance Across the Flight Envelope”. Mr. John Bosworth is the Technical Monitor. Additionally, it is supported by the National Science Foundation under Grant No. NSF-CMMI-1254129 entitled “CAREER: Probabilistic Tools for High Reliability Monitoring and Control of Wind Farms”.

References

[1] D. Bates and I. Postlethwaite,eds. "Robust multivariable control of aerospace systems". Vol. 8, IOS Press, 2002.

[2] J. Beranek, L. Nicolai, M. Buonanno, E. Burnett, C. Atkinson, B. Holm-Hansen and P. Flick. "Conceptual design of a multi-utility aeroelastic demonstrator". *13th AIAA/ISSMO Multidisciplinary Analysis Optimization Conference*, Vol. 3, 2010.

[3] J. D. Blight, R. Lane Dailey and D. Gangsaas. "Practical control law design for aircraft using multivariable techniques". *International Journal of Control*, Vol. 59, pp. 93-137, 1994.

[4] F. Demourant "New algorithmic approach based on integral quadratic constraints for stability analysis of high order models". *In Proceedings of the European Control Conference*, pp. 359-364, 2013.

[5] C. A. Desoer and M. Vidyasagar. "Feedback systems: input-output properties". Vol. 55, Siam, 2009.

[6] A. Megretski and A. Rantzer. "System analysis via integral quadratic constraints". *IEEE Transactions on Automatic Control*, Vol. 42, pp. 819-830, 1997.

[7] A. Packard and J. Doyle. "The complex structured singular value". *Automatica*, Vol. 29, pp. 71-109, 1993.

[8] H. Pfifer and B. Danowsky. "System Identification of a Small Flexible Aircraft". *In Proceedings of the AIAA SciTech Conference*, 2016.

[9] H. Pfifer and P. Seiler. "Integral quadratic constraints for delayed nonlinear and parameter-varying systems". *Automatica*, Vol. 56, pp. 36-43, 2015.

[10] H. Pfifer and P. Seiler. "Robustness analysis of linear parameter varying systems using integral quadratic constraints". *International Journal of Robust and Nonlinear Control*, Vol. 25, pp. 2843-2864, 2015.

[11] H. Pfifer and P. Seiler. "Less conservative robustness analysis of linear parameter varying systems using integral quadratic constraints". *International Journal of Robust and Nonlinear Control*, 2016.

[12] M. G. Safonov. "Stability and robustness of multivariable feedback systems". MIT Press, 1980.

[13] C. Scherer, I. Kose. "Gain-Scheduled Control Synthesis Using Dynamic-Scales". *IEEE Transactions on Automatic Control*, Vol. 57, pp 2219-2234, 2012.

[14] D.K. Schmidt, W. Zhao and R.K. Kapania. "Flight-Dynamics and Flutter Modeling and Analysis of a Flexible Flying-Wing Drone". *In Proceedings of the AIAA SciTech Conference*, pp. 4-8, 2016.

[15] J. Theis, H. Pfifer and P. Seiler. "Robust Control in Flight: Active Flutter Suppression". *In Proceedings of the AIAA Science and Technology Forum*, 2016.

[16] J. Veenman, K. Hakan , and C. W. Scherer. "Analysis of the controlled NASA HL20 atmospheric re-entry vehicle based on dynamic IQCs". *In AIAA Guidance, Navigation and Control Conference*, 2009.

[17] M.R. Waszak and D.K. Schmidt. "Flight dynamics of aeroelastic vehicles". *Journal of Aircraft*, Vol. 25, pp. 563-571, 1988.

[18] F. Wu. "Control of linear parameter varying systems". Doctoral dissertation, University of California at Berkeley, 1995.

[19] F. Wu, X.H. Yang, A. Packard and G. Becker. "Induced L2-norm control for LPV system with bounded parameter variation rates". *American Control Conference*, Vol. 3 IEEE, pp. 2379-2383, 1995.

[20] K. Zhou, J.C. Doyle and K. Glover. "Robust and optimal control". Vol. 40, New Jersey: Prentice hall, 1996.